A Self-Synchronized Decentralized Control for Series-Connected H-Bridge Rectifiers

Hou, X.; Sun, Y.; Zhang, X.; Zhang, G.; Lu, J.; Blaabjerg, Frede

Published in:
IEEE Transactions on Power Electronics

DOI (link to publication from Publisher):
10.1109/TPEL.2019.2896150

Publication date:
2019

Document Version
Accepted author manuscript, peer reviewed version

This article has been accepted for publication in a future issue of this journal, but has not been fully edited. Content may change prior to final publication. Citation information: DOI 10.1109/TPEL.2019.2896150, IEEE Transactions on Power Electronics

A Self-Synchronized Decentralized Control for Series-Connected H-bridge Rectifiers

Xiaochao Hou, *Student Member, IEEE*, Yao Sun, *Member, IEEE*, Xin Zhang, *Member, IEEE*, Guanguan Zhang, *Member, IEEE*, Jinghang Lu, *Member, IEEE*, and Frede Blaabjerg, *Fellow, IEEE*

[1]***Abstract*—This study proposes a decentralized coordination control scheme for series-connected H-bridge rectifiers. Each rectifier module is controlled as a voltage-controlled source by a local controller, which needs only individual information. The local controller is composed of an active power-frequency (P-ω) control and a fixed voltage amplitude control. Compared to the conventional methods based multi-level phase-shifting modulation where centralized controller is needed, the proposed control strategy allows indefinite modular expansion without increasing the computational load of the local controller. Therefore, it has decreased cost and increased scalability. The synchronization mechanism of series modules is analyzed and the stability of the system is proved. The feasibility of the proposed strategy is verified by experimental results.**

***Index Terms*—Decentralized control, scalability, series-connected rectifiers, self-synchronization;**

I. Introduction

Series-type converters have been a promising solution to the high-voltage power conversion system due to their modularity, transformer-less feature and high power quality. They have been widely studied in the cascaded photovoltaic micro-inverters [1], high-voltage reactive power compensation [2] and the applications of electrical traction, vehicle-to-grid and solid-state transformer [3]-[5]. In the application of solid-state transformer, series-type converters work in rectifier mode.

The existing researches [3]-[6] mostly focus on the multi-level modulation techniques of series-connected rectifiers to obtain sinusoidal input current, adjustable power factor, dc-link voltage regulation, and ac grid voltage synchronization. In [3], an innovative modulation technique of synthesizing multiple control loops is developed to strictly balance the dc capacitor and ensure a quasi-sinusoidal grid current. In [4], a unified voltage balance control is proposed to overcome the uncertain power flow direction and unbalance power sharing of series modules. Particularly, some improved modulation mechanisms are proposed for unbalanced compensation [5] and neutral-point potential balancing [6]. Although these modulation-based methods have good performances, all computational burden is undertaken by a central controller processor. As the number of rectifier modules increases, the computational complexity increases exponentially, which decreases reliability and limits its application scale.

Recently, decentralized coordination control of modular converters has become popular because of its high reliability and flexibility. In [7] and [8], a general decentralized control strategy is proposed for four series-parallel dc/dc conversion architectures to guarantee autonomous voltage and power balance. Then, the idea of decentralized control is extended to modular dc/ac inverters, including typical input-series-output-parallel [9] and input-series-output-series ones [10]. As input and output powers of each inverter module are coupled and balanced, achieving input-dc-voltage-balance means output-power-balance automatically. Different from [9] and [10], literature [11] uses frequency self-synchronization control to achieve decentralized power balance in series-connected inverters. However, its stability highly depends on the load characteristic and only the resistive-inductive load is applicable. To overcome this limitation, an adaptive droop control is proposed in [12], where the proposed control basically becomes an inverse droop control under resistive-inductive load and a droop control under the resistive-capacitive load. However, the aforementioned [11]-[12] only focus on islanded mode of series-connected inverters. Whereas, series-connected inverters working in rectifier operation of grid-connected mode has not been studied before.

To fill the gap, this study proposes a fully decentralized control for series-connected rectifiers. It realizes the autonomous voltage balance and frequency synchronization among modules. As a result, central controller is not necessary to coordinate the balance control for individual modules. Thus, the proposed method is suitable for an arbitrary number of series modules. Compared to the central modulation-based schemes [3]-[6], the proposed method has the features:

- *Coordination-control-based for modular rectifiers.* A decentralized control is proposed to coordinate all modules instead of the central modulation-based method.
- *Voltage-controlled rectifier module.* In this work, each rectifier module is controlled as a voltage source, including the frequency-synchronization control and voltage control.
- *High scalability and low cost.* As there is not a complex communication network, the proposed control improves the scalability and decreases the cost.

[1] Manuscript received November 22, 2018; revised January 9, 2019; accepted January 22, 2019. This work was supported in part by the National Natural Science Foundation of China under Grant 61622311, the Joint Research Fund of Chinese Ministry of Education under Grant 6141A02033514, the Project of Innovation-driven Plan in Central South University under Grant 2019CX003, the Major Project of Changzhutang Self-dependent Innovation Demonstration Area under Grant 2018XK2002, and the Hunan Provincial Innovation Foundation for Postgraduate under Grant CX2018B060. *(Corresponding author: Yao Sun.)*

X. Hou and Y. Sun are with the Hunan Provincial Key Laboratory of Power Electronics Equipment and Grid, School of Automation, Central South University, Changsha 410083, China (e-mail: houxc10@csu.edu.cn; yaosuncsu@gmail.com).

X. Zhang and J. Lu are with the School of Electrical and Electronic Engineering, Nanyang Technological University, Singapore 639798 (e-mail: jackzhang@ntu.edu.sg; lujh@ntu.edu.sg).

G. Zhang is with the School of Control Science and Engineering, Shandong University, Jinan, China (e-mail: dr_zgg@163.com).

F. Blaabjerg is with the Department of Energy Technology, Aalborg University, DK-9220 Aalborg, Denmark (e-mail: fbl@et.aau.dk).

This article has been accepted for publication in a future issue of this journal, but has not been fully edited. Content may change prior to final publication. Citation information: DOI 10.1109/TPEL.2019.2896150, IEEE Transactions on Power Electronics

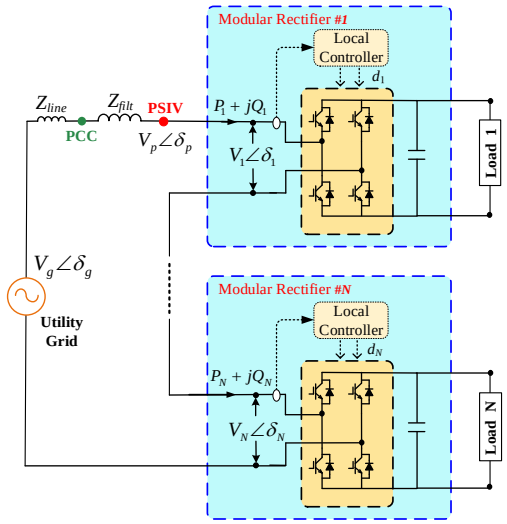

Fig. 1. Topology of series-connected rectifier modules.

II. Decentralized Control for Series Rectifiers

A. Models of Series-Connected Rectifiers

Fig. 1 shows the basic topology of series-connected rectifiers, which consists of N series-connected H-bridge modules. On the ac side, there is a filter inductance Z_{filt} between the point of common coupling (PCC) and rectifiers. On the dc side, each rectifier module has an independent dc-link capacitor and an isolated load. In this study, we focus on the series-connected rectifiers with the same power demand. In practice, it is very common in solid-state transformers and traction applications [3]-[5].

In Fig.1, each rectifier module is controlled by an independent local controller, and the input characteristic of each module is equivalently treated as a voltage-controlled source. Then, the absorbed real power P_i and reactive power Q_i of *i-th* module from the utility grid (UG) are given by

$$P_i + jQ_i = V_i e^{j\delta_i} \cdot \left((V_g e^{j\delta_g} - V_p e^{j\delta_p}) / (|Z_f| e^{j\theta_f}) \right)^* \quad (1)$$

where V_i and δ_i represent the fundamental-frequency input voltage amplitude and phase angle of *i-th* module. V_g and δ_g are the voltage amplitude and phase angle of UG. $|Z_f|$ and θ_f are the amplitude and angle of the total grid impedance, including filter impedance Z_{filt} and line impedance Z_{line}.

The voltage at point of stacked input-voltage (PSIV) of modular rectifiers is the sum of all module input-voltages.

$$V_p e^{j\delta_p} = \sum_{j=1}^{N} V_j e^{j\delta_j} \quad (2)$$

Generally, the total grid impedance is mainly inductive ($\theta_f \approx \pi/2$). In this case, the power transmission characteristic is given by

$$P_i = \frac{V_i}{|Z_f|}\left(\sum_{j=1}^{N} V_j \sin(\delta_i - \delta_j) - V_g \sin(\delta_i - \delta_g) \right) \quad (3)$$

$$Q_i = \frac{V_i}{|Z_f|}\left(V_g \cos(\delta_i - \delta_g) - \sum_{j=1}^{N} V_j \cos(\delta_i - \delta_j) \right) \quad (4)$$

B. Proposed Decentralized Control

To synchronize each module with UG and flexibly control the absorbed active power, a decentralized control scheme is proposed

$$\begin{cases} \omega_i = \omega^* + k \cdot (P_i - P_i^*) \\ V_i = V^* \end{cases} \quad (5)$$

where ω_i and V_i are the angular frequency and voltage amplitude references of *i-th* module, respectively. ω^* represents the nominal value of grid angular frequency. k is a positive gain of P-ω control. V^* is a predesigned voltage parameter related to grid power factor and system stability, which will be assigned later. P_i^* represents the power reference absorbed from the grid, which is constructed as follow to balance the DC-link capacitor voltage V_{dci}.

$$P_i^* = P_0 + (k_p + \frac{k_I}{s})(V_{dc}^* - V_{dci}) \quad (6)$$

where k_p and k_I are the proportional-integral (PI) coefficients. V^*_{dc} is the dc-link voltage reference for each module. P_0 is a feed-forward power compensation term, which only impacts on the system startup dynamic. Generally, P_0 is equal to the rated load power. In steady-state, the control objective of (6) is to balance the DC-link capacitor voltage which is a favorable indication of load demand.

According to (5)-(6), the voltage-controlled control diagram of *i-th* rectifier module is presented in Fig. 2. The voltage-generation reference is indicated by combining the voltage amplitude V^* and phase angle δ_i. The input active power is calculated based on the input current sampling and inner voltage-generation reference. It is noted that the notch filter is implemented to attenuate the twice line-frequency ripple of dc-link voltage in the control loop [13].

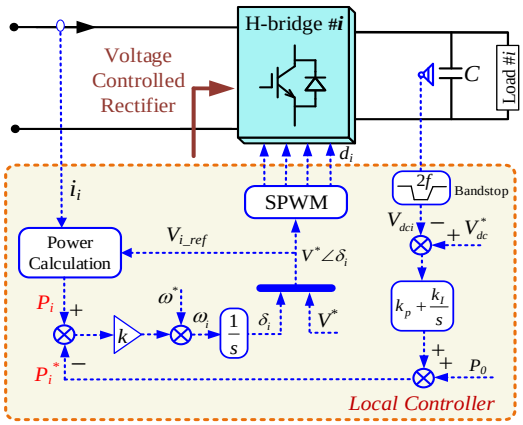

Fig. 2. The local controller of *i-th* voltage-controlled rectifier module.

C. Steady-State Analysis

In steady state, as the voltage amplitude V^* is same for all rectifiers and each module shares the same grid current, their apparent powers are equal.

$$S_1 = S_2 = \cdots = S_N \quad (7)$$

As the active powers of all DC-links feeding loads are the same, (8) is obtained from (5) due to the identical grid frequency ($\omega_1 = \cdots = \omega_N = \omega^*$)

$$P_1 = P_2 = \cdots = P_N = P^* \quad (8)$$

From (7)-(8), it can be deduced that the phase angles of all modules are equal in the steady state ($\delta_i = \delta_j$; $i,j \in \{1,2 \ldots N\}$). Further, the voltage at PSIV is derived from (2)

This article has been accepted for publication in a future issue of this journal, but has not been fully edited. Content may change prior to final publication. Citation information: DOI 10.1109/TPEL.2019.2896150, IEEE Transactions on Power Electronics

$$V_p = NV^*; \quad \delta_p = \delta_1 = \delta_2 \cdots = \delta_N \tag{9}$$

From (3)-(4), the steady state power of each module is given

$$\bar{P}_i = P^* = -S_C \sin\bar{\delta}; \quad \bar{Q}_i = S_C\left(\cos\bar{\delta} - NV^*/V_g\right) \tag{10}$$

where $S_C = \left(V_g V^*/|Z_f|\right)$ represents the active power transfer capacity of a single module. $\bar{\delta} = (\delta_p - \delta_g)$ refers to the steady power angle. From (10), two steady points exist: $\bar{\delta} = -\arcsin(\frac{P^*}{S_C})$ or $\bar{\delta} = \pi + \arcsin(\frac{P^*}{S_C})$.

Then, the voltage amplitude reference V^* is designed according to the required grid power factor from (10) as $\tan\phi = \left(\bar{Q}_i/\bar{P}_i\right)$.

$$V^* = \frac{V_g}{N}(\tan\phi\sin\bar{\delta} + \cos\bar{\delta}) \tag{11}$$

where ϕ is the predesigned grid power factor angle.

For a given power factor in (11), V^* can be calculated if the total grid impedance is known. Normally, filter impedance is pre-designed and easily known, and line impedance can be negligible when filter impedance is far greater than line impedance ($|Z_{filt}|>>|Z_{line}|$). However, for a weak grid, line impedance profiles should be measured with the frequency scanning technique [14]-[15].

D. Synchronization Mechanism Analysis

For a better understanding of the proposed control, the frequency synchronization mechanism of series modules is illustrated in Fig. 3. For simplicity, we assume two rectifier modules in series. The equivalent circuit and phasor diagrams are given in Fig. 3(a) and Fig. 3(b), respectively.

In Fig. 3(b), V_1 (*green phasor*) leads the steady-state voltage (*red phasor*); while V_2 *(blue phasor)* lags it. As two modules have the same voltage amplitude V^* and the same grid current I_g, their apparent powers are equal all the time (S_1=S_2). Initially, $\delta_1>\delta_2$, $P_1<P^*<P_2$. Then, $\omega_1<\omega^*<\omega_2$ is obtained from (5). As a result, δ_1 decreases ($\Delta\omega_1=\omega_1-\omega^*<0$), while δ_2 increases ($\Delta\omega_2=\omega_2-\omega^*>0$). The convergence process will continue until $\delta_1=\delta_2$, $\omega_1=\omega_2=\omega^*$, and $P_1=P_2=P^*$.

It is worth noting that the synchronization mechanism of series modules is totally different from that of parallel converters. In the series modules, active power control is essentially a power factor control as the same flowing current and $P=V^*I\cos\phi$ [16]. While for the parallel modules, active power control is a power angle control as $P=\frac{V_1V_2}{X}\sin\delta$, where δ denotes the power angle of power transmission [17].

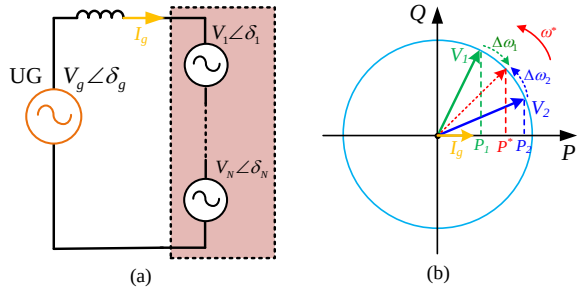

Fig. 3. A simplified series-connected rectifiers system for synchronization mechanism analysis. (a) Equivalent circuit, (b) phasor diagram.

III. Stability Proof of Frequency Synchronization

Stability is essential for the normal operation of the series-connected rectifiers. Thus the small signal stability analysis for the system is carried out in this section.

First, the dynamic model of the DC capacitor is built.

$$C\frac{dV_{dci}}{dt} = \frac{P_i}{V_{dci}} - \frac{V_{dci}}{R_{load}} \tag{12}$$

where C is the value of DC capacitor. R_{load} implies an equivalent resistor of the load demand.

Then, linearizing (3), (5), (6) and (12) around the steady state points yields

$$\begin{cases} \tilde{P}_i = \dfrac{V^*}{|Z_f|}\left(\sum_{j=1,j\neq i}^{N} V^*\left(\tilde{\delta}_i - \tilde{\delta}_j\right) - V_g(\cos\bar{\delta})\left(\tilde{\delta}_i - \tilde{\delta}_g\right)\right) \\ \dot{\tilde{\delta}}_i = \tilde{\omega}_i = k\cdot(\tilde{P}_i - \tilde{P}_i^*); \quad \tilde{P}_i^* = -k_p\tilde{V}_{dci} - k_I\tilde{\Phi}_{dci} \\ \dot{\tilde{\Phi}}_{dci} = \tilde{V}_{dci}; \quad \dot{\tilde{V}}_{dci} = \dfrac{1}{V_{dc}^*C}\tilde{P}_i - \dfrac{P^*}{V_{dc}^{*2}C}\tilde{V}_{dci} - \dfrac{1}{R_{load}C}\tilde{V}_{dci} \end{cases} \tag{13}$$

where '~' denotes small perturbation around equilibrium points.

Rewrite (13) in matrix form as

$$\begin{bmatrix} \dot{\tilde{\delta}} \\ \dot{\tilde{\Phi}}_{dc} \\ \dot{\tilde{V}}_{dc} \end{bmatrix} = [A_s]_{3N\times 3N}\begin{bmatrix} \tilde{\delta} \\ \tilde{\Phi}_{dc} \\ \tilde{V}_{dc} \end{bmatrix} = \begin{bmatrix} -kh_1A_1 & kk_II & kk_pI \\ 0 & 0 & I \\ -h_3h_1A_1 & 0 & -h_4I \end{bmatrix}\begin{bmatrix} \tilde{\delta} \\ \tilde{\Phi}_{dc} \\ \tilde{V}_{dc} \end{bmatrix} \tag{14}$$

where

$$\begin{cases} \tilde{\delta} = \begin{bmatrix}\tilde{\delta}_1 & \tilde{\delta}_2 & \cdots & \tilde{\delta}_N\end{bmatrix}^T;\ \tilde{\Phi}_{dc} = \begin{bmatrix}\tilde{\Phi}_{dc1} & \tilde{\Phi}_{dc2} & \cdots & \tilde{\Phi}_{dcN}\end{bmatrix}^T \\ \tilde{V}_{dc} = \begin{bmatrix}\tilde{V}_{dc1} & \tilde{V}_{dc2} & \cdots & \tilde{V}_{dcN}\end{bmatrix}^T;\ A_1 = h_2I + 1_N1_N^T \\ h_1 = \dfrac{V^{*2}}{|Z_f|};\ h_2 = \dfrac{V_g\cos\bar{\delta}}{V^*} - N;\ h_3 = \dfrac{1}{V_{dc}^*C};\ h_4 = \dfrac{P^*}{V_{dc}^{*2}C} + \dfrac{1}{R_{load}C} \end{cases} \tag{15}$$

The system stability is analyzed by inspecting the eigenvalues of matrix A_s, which are obtained by solving (16).

$$|\lambda I - A_s| = \left|\lambda^3 I + \lambda^2(h_4I + kh_1A_1) + \lambda(h_4 + k_ph_3)kh_1A_1 + kk_Ih_1h_3A_1\right| = 0 \tag{16}$$

In (16), since the matrix A_1 is symmetric and diagonalizable, then there exists a nonsingular matrix Z to meet

$$\begin{aligned} &\left|Z^{-1}(\lambda^3 I + \lambda^2(h_4I + kh_1A_1) + \lambda(h_4 + k_ph_3)kh_1A_1 + kk_Ih_1h_3A_1)Z\right| \\ &= \left|\lambda^3 I + \lambda^2(h_4I + kh_1\Lambda) + \lambda(h_4 + k_ph_3)kh_1\Lambda + kk_Ih_1h_3\Lambda\right| = 0 \end{aligned} \tag{17}$$

where $Z^{-1}A_1Z = \Lambda = diag\{\mu_i\};\ \ i\in\{1,2,\cdots,N\}$.

Then, the 3N-order polynomial equation is decomposed into N cubic equations as

$$\lambda^3 + \lambda^2(h_4 + kh_1\mu_i) + \lambda(h_4 + k_ph_3)kh_1\mu_i + kk_Ih_1h_3\mu_i = 0;\ i\in\{1,2,\cdots,N\} \tag{18}$$

According to Routh-Hurwitz criterion, the necessary and sufficient conditions of system stability are obtained from (18)

$$\begin{cases} h_4 + kh_1\mu_i > 0; \quad (h_4 + k_ph_3)kh_1\mu_i > 0 \\ kk_Ih_1h_3\mu_i > 0 \qquad\qquad\qquad\qquad ;\ i\in\{1,2,\cdots,N\} \\ (h_4 + kh_1\mu_i)(h_4 + k_ph_3)kh_1\mu_i > kk_Ih_1h_3\mu_i \end{cases} \tag{19}$$

From (15), the eigenvalues of the matrix A_1 are given by

$$\mu_1 = \frac{V_g\cos\bar{\delta}}{V^*}; \quad \mu_2 = \cdots = \mu_N = \frac{V_g\cos\bar{\delta}}{V^*} - N. \tag{20}$$

This article has been accepted for publication in a future issue of this journal, but has not been fully edited. Content may change prior to final publication. Citation information: DOI 10.1109/TPEL.2019.2896150, IEEE Transactions on Power Electronics

As the constants h_1, h_3, h_4 in (15) are greater than zero, the stability conditions are simplified from (19)-(20) as follows

$$\begin{cases} \cos\bar{\delta} > 0 \\ k > 0 \\ V_g \cos\bar{\delta} - NV^* > 0 \\ k_p > -(h_4/h_3); \quad (h_4 + kh_1h_2)(h_4/h_3 + k_p) > k_I > 0 \end{cases} \tag{21}$$

From the analysis above, we could conclude that:

1) As $\cos\bar{\delta} > 0$, the power angle $\bar{\delta}$ should lie in (-π/2, π/2) in steady state. Thus, only $\bar{\delta} = -\arcsin(P^*/S_c)$ is the stable equilibrium point in (10), and $\bar{\delta}$ is normally around 0, which indicates $\cos\bar{\delta} \cong 1$.
2) From (21), the *P*-ω control gain *k* must be positive for grid-connected series rectifiers, which is different with the islanded series-connected inverters [12]. Moreover, a fast convergence rate of the frequency dynamic can be obtained by increasing *k* from (18). But a too large *k* will cause unacceptable frequency overshoots. Thus, a proper *k* could be designed by making a compromise between settling time and overshoot.
3) In (21), the predesigned voltage amplitude V^* should meet $V^* < (V_g \cos\bar{\delta}/N)$ for system stability. From (11), a high power factor requires that V^* is close to the stability upper bound $(V_g \cos\bar{\delta}/N)$. However, a high value V^* is detrimental to stability from (21). Thus, a proper V^* should be designed by making a tradeoff between power factor requirement and stability margin.
4) For stability, the selection of PI coefficients k_p and k_I of dc-link capacitor control should meet (21).

IV. Discussion of Proposed Control Strategy

A. Discussion of Proposed Control in Abnormal Condition

According to the stability condition $V_g > NV^*$ in (21), if control parameters are properly set, the system would be stable in normal grid condition and the cases where there are grid voltage swell and small grid voltage dip. However, when a large grid dip occurs, and the condition is not further satisfied, the additional measures should be adopted.

Two potential measures can be taken. In the first one, a dynamic voltage regulator (DVR) can be series-connected with utility grid to guarantee a normal grid voltage [18]. In the second one, we could modify the voltage reference V_i by adding a feed-forward compensation to (5):

$$V_i = V^* + \frac{V_g - V_g^*}{N} \tag{22}$$

where V_g and V_g^* are measured voltage amplitude and nominal amplitude of grid voltage. If each module samples the grid voltage, the cost will increase. Another method is to use communication to acquire V_g. As V_g is a slow variable, a low-bandwidth communication is needed, such as an optical fiber with a 5 Mb/s execution speed [19], [20].

B. Comparisons with Existing Methods

Table I presents a comparison between the centralized methods and the proposed decentralized method. Compared to the centralized methods, the superior feature of the proposed decentralized method is the self-synchronization, and it makes it possible for an arbitrary number of series modules. However, the proposed method has lower performances of disturbance rejection ratio and resilient to grid dynamic. Moreover, as only the grid voltage amplitude is acquired via a distributed low-bandwidth communication, the transfer data latency and communication burden of the proposed control strategy are significantly reduced.

TABLE I
COMPARISON WITH THE EXISTING METHODS

Features	Centralized methods [3]-[6]	Proposed decentralized method
Synchronization method	Centralized communication	Self-synchronization
Communication bandwidth	High	Low
Cost	High	Low
Complexity	High	Low
Resilient to communication failure	Low	High
Resilient to grid dynamic	High	Low
Disturbance rejection ratio	High	Low
Scalability	Low	High
Application scale	Limited	Arbitrary

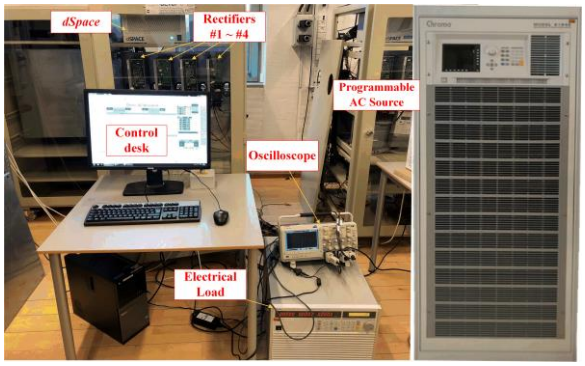

Fig. 4. Picture of the experimental setup.

TABLE II
EXPERIMENTAL PARAMETERS

Symbol	Value	Symbol	Value	Symbol	Value
Physical parameters					
V_g	311 V	ω^*	2π*50 rad/s	P_0	2 kW
C	3300 μF	Z_f	0.08+j1.0 Ω	R_{load}	20 Ω
Control parameters					
k	1.2e-4	k_p/k_I	8/8	V^*_{dc}	200 V
N	4	$\cos\phi$	0.995	V^*	75

V. Experimental Results

To verify the feasibility of the proposed control scheme, a system comprised of four series-connected rectifier modules has been built and tested in the lab. A picture of the experimental setup is shown in Fig. 4. The dSPACE1006 platform is used for controlling series rectifiers, and the waveforms of the electrical quantities are recorded by the oscilloscope. The system parameters are designed according to steady-state analysis (11) and stability condition (21) as listed in Table II. The switching frequency of rectifiers is 10 kHz. Moreover, beyond the research of this work, a power decoupling technology is used to suppress the twice line

This article has been accepted for publication in a future issue of this journal, but has not been fully edited. Content may change prior to final publication. Citation information: DOI 10.1109/TPEL.2019.2896150, IEEE Transactions on Power Electronics

frequency ripple of DC capacitor in single-phase systems [13].

A. Performances under Normal-Grid Condition

Fig.5 and Fig. 6 show the experimental results in normal-grid condition. From the voltage/current waveforms at utility grid in Fig. 5, a sinusoidal input current is guaranteed and a predesigned power factor 0.995 is enabled. Moreover, the system achieves real-power/reactive-power balances among four modules in Fig. 6(a)-(b), autonomous grid frequency synchronization in Fig. 6(c), equal DC capacitor voltage balances in Fig. 6(d) in steady-state. Meanwhile, the DC-link capacitor voltage is maintained at the desired value 200 V, and has a satisfactory response and good stability.

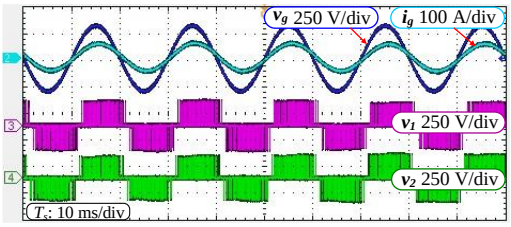

Fig. 5. Results under normal-grid condition. (From top to down: grid voltage v_g, grid current i_g, input voltage v_1~v_2 of module#1 and module#2).

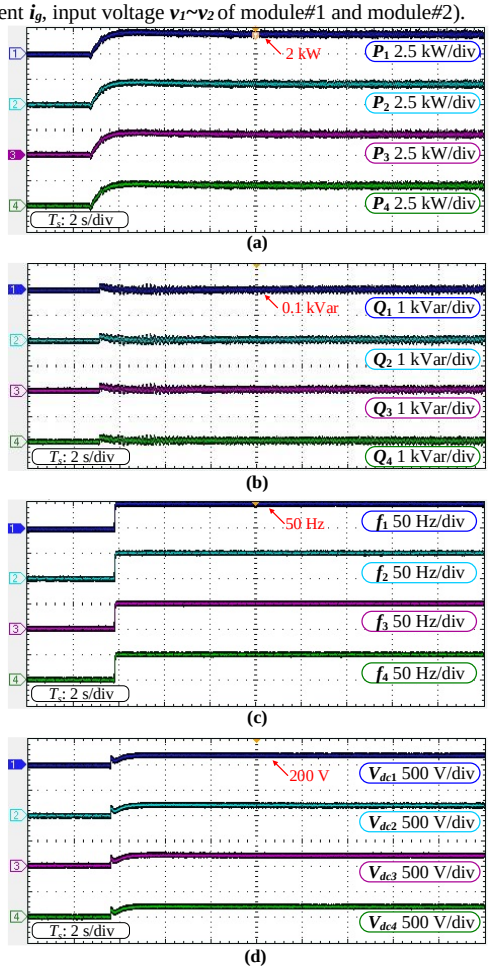

Fig. 6. Results of four modules under normal-grid condition. (a) Input active power P_1~P_4, (b) input reactive power Q_1~Q_4, (c) operation frequency f_1~f_4, and (d) DC-link capacitor voltage V_{dc1}~ V_{dc4}.

B. Performances under Load Change

This case study aims to evaluate the response of the proposed control strategy under different load power levels. The experimental results are shown in Fig. 7 and Fig. 8. The four dc-link resistance loads of rectifiers are simultaneously changed from 2 kW to 1kW at t=2s.

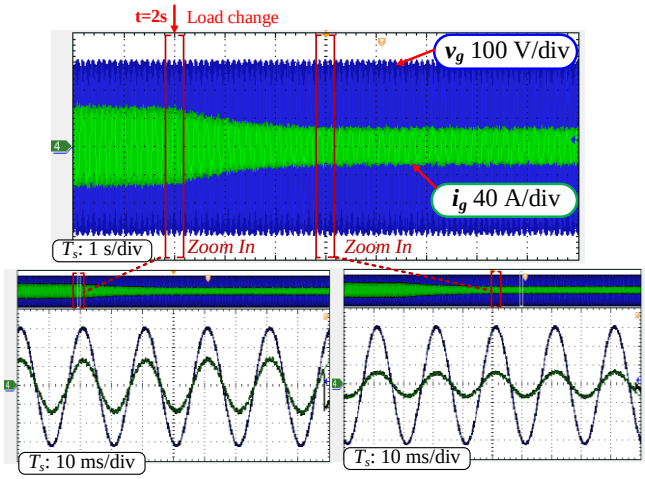

Fig. 7. Grid voltage v_g and grid current i_g waveforms under load change.

Fig.7 shows the grid voltage and current waveforms before and after the load change. Clearly, the grid current of P^*=2 kW is twice as large as the grid current of P^*=1 kW. From fig. 8, the active power, reactive power and dc-link capacitor voltage of four modules reach the new steady-state after a regulation time of about two seconds. The dynamic response is smooth and satisfactory.

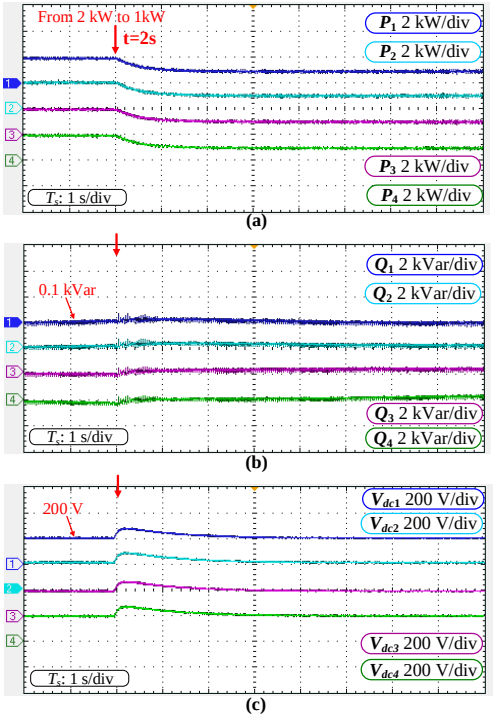

Fig. 8. Results of four modules under load change. (a) Input active power P_1~P_4, (b) input reactive power Q_1~Q_4, and (c) DC-link capacitor voltage V_{dc1}~ V_{dc4}.

C. Performances under 2% Grid Voltage Dip

In this case, a small grid disturbance is considered to verify the effectiveness of the proposed decentralized control scheme without adopting (22). Fig. 9 shows the experimental results. According to the IEC 61000 standard, a 2% grid voltage dip is imposed at t=3s as shown in Fig. 9(a). For the dynamic response, the grid current and input active powers are almost unaffected. Only the reactive powers have a slight decrease.

This article has been accepted for publication in a future issue of this journal, but has not been fully edited. Content may change prior to final publication. Citation information: DOI 10.1109/TPEL.2019.2896150, IEEE Transactions on Power Electronics

On the whole, the proposed method of (5) is still feasible under a small grid disturbance, which verifies the analysis and discussion of section V.

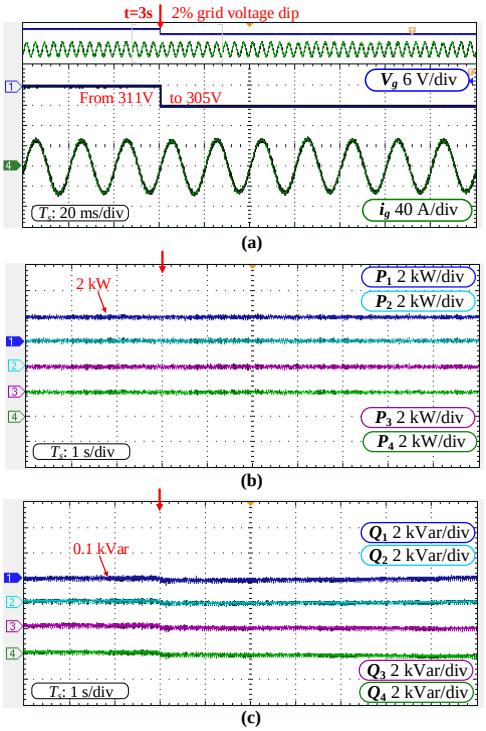

Fig. 9. Results under 2% grid voltage dip. (a) Grid voltage amplitude V_g, grid current i_g, (b) input active power P_1~P_4, and (c) input reactive power Q_1~Q_4.

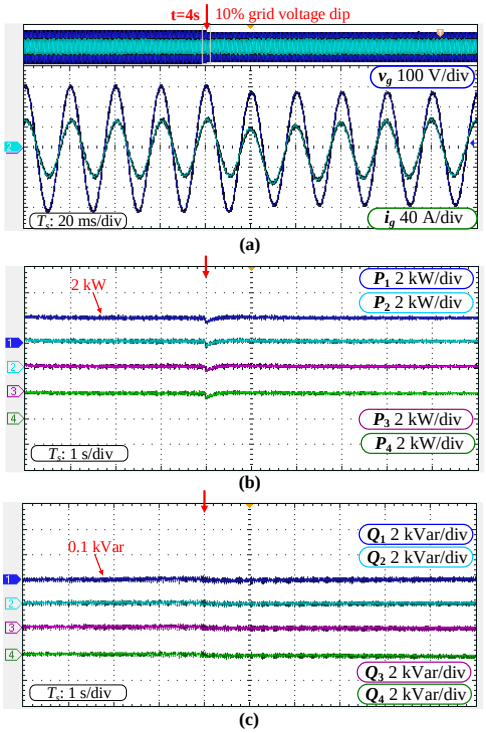

Fig. 10. Results under 10% grid voltage dip. (a) Grid voltage v_g, grid current i_g, (b) input active power P_1~P_4, and (c) input reactive power Q_1~Q_4.

D. Performances under 10% Grid Voltage Dip

For a large grid disturbance, the experimental test under abnormal grid condition is conducted to verify the proposed decentralized control of (5) and (22). Fig. 10 shows the experimental results. A 10% grid voltage dip is imposed at t=4s as shown in Fig. 10(a).

Initially, grid voltage is normal, and all modules work normally during t=0s-4s. When the grid voltage dip occurs, the system does not lose stability, and only active power has a small impulse. With the function of grid-voltage feed-forward, the system returns to be normal after about five cycles in Fig. 10(a). From this case, the proposed control method can still work in the large grid disturbance condition.

VI. Conclusion

This study exploits a novel decentralized control concept for series-connected H-bridge rectifiers. It realizes autonomous frequency synchronization and DC-link voltage regulation. Because all control tasks are assigned to local controllers, the centralized high-bandwidth communication is avoided. Consequently, the transfer data latency and communication burden of proposed control strategy are significantly reduced, and the flexible scalability is greatly enhanced compared with the centralized control. These characteristics would promote potential applications of the proposed control strategies in solid-state transformers and vehicle-to-grid.

VII. References

[1] H. D. Tafti, A. I. Maswood, G. Konstantinou, C. D. Townsend, P. Acuna, and J. Pou, "Flexible control of photovoltaic grid-connected cascaded H-bridge converters during unbalanced voltage sags," *IEEE Trans. Ind. Electron.*, vol. 65, no. 8, pp. 6229-6238, Aug. 2018.

[2] X. Hou, Y. Sun, H. Han, Z. Liu, M. Su, B. Wang, and X. Zhang, "A general decentralized control scheme for medium-/high-voltage cascaded STATCOM," *IEEE Trans. Power Systems*, vol. 33, no. 6, pp. 7296-7300, Nov. 2018.

[3] C. Cecati, A. D. Aquila, M. Liserre, and V. G. Monopoli, "Design of H-bridge multilevel active rectifier for traction systems," *IEEE Trans. Ind. Appl.*, vol. 39, no. 5, pp. 1541–1550, Sep./Oct. 2003.

[4] D. Sha, G. Xu and Y. Xu, "Utility direct interfaced charger/discharger employing unified voltage balance control for cascaded H-bridge units and decentralized control for CF-DAB modules," *IEEE Trans. Ind. Electron.*, vol. 64, no. 10, pp. 7831-7841, Oct. 2017.

[5] L. Wang, D. Zhang, Y. Wang, B. Wu, and H. S. Athab, "Power and voltage balance control of a novel three-phase solid-state transformer using multilevel cascaded H-bridge inverters for microgrid applications," *IEEE Trans. Power Electron.*, vol. 31, no. 4, pp. 3289–3301, Apr. 2016.

[6] K. Sun, X. Lin, Y. Li, Y. Gao and L. Zhang, "Improved modulation mechanism of parallel-operated T-Type three-level PWM rectifiers for neutral-point potential balancing and circulating current suppression," *IEEE Trans. Power Electron.*, vol. 33, no. 9, pp. 7466-7479, Sept. 2018.

[7] W. Chen, X. Ruan, H. Yan and C. K. Tse, "DC/DC conversion systems consisting of multiple converter modules: stability, control, and experimental verifications," *IEEE Trans. Power Electron.*, vol. 24, no. 6, pp. 1463-1474, June 2009.

[8] G. Xu, D. Sha, and X.Liao, "Decentralized inverse-droop control for input-series-output-parallel DC-DC converters," *IEEE Trans. Power Electron.*,vol. 30, no. 9, pp. 4621–4625, Sep. 2015.

[9] L. Shu, W. Chen and X. Jiang, "Decentralized control for fully modular input-series-output-parallel (ISOP) inverter system based on the active power inverse-droop method," *IEEE Trans. Power Electron.*, vol. 33, no. 9, pp. 7521-7530, Sept. 2018.

[10] D. Sha, G. Xu and X. Liao, "Control strategy for input-series-output-series high-frequency AC-link inverters," *IEEE Trans. Power Electron.*, vol. 28, no. 11, pp. 5283-5292, Nov. 2013.

[11] J. He, Y. Li, B. Liang and C. Wang, "Inverse power factor droop Control for decentralized power sharing in series-connected-microconverters-based islanding microgrids," *IEEE Trans. Ind. Electron.*, vol. 64, no. 9, pp. 7444-7454, Sept. 2017.

[12] Y. Sun, G. Shi, X. Li, W. Yuan, M. Su, H. Han, and X. Hou, "An f-P/Q droop control in cascaded-type microgrid," *IEEE Trans. Power Systems*, vol. 33, no. 1, pp. 1136-1138, Jan. 2018.

[13] Y. Sun, Y. Liu, M. Su, W. Xiong and J. Yang, "Review of Active Power Decoupling Topologies in Single-Phase Systems," *IEEE Trans.Power Electronics*, vol. 31, no. 7, pp. 4778-4794, Jul. 2016.

[14] X. Wang and F. Blaabjerg, "Harmonic Stability in Power Electronic Based Power Systems: Concept, Modeling, and Analysis," in *IEEE Transactions on Smart Grid*, 2018. Doi: 10.1109/TSG.2018.2812712.
[15] P. M. Anderson, B. L. Agrawal, and J. E. Van Ness, *Subsynchronous Resonance in Power Systems*, New York: IEEE Press, 1990.
[16] X. Hou, Y. Sun, H. Han, Z. Liu, W. Yuan and M. Su, "A fully fecentralized control of grid-connected cascaded inverters," *IEEE Trans. Sustainable Energy*, vol. 10, no. 1, pp. 315-317, Jan. 2019.
[17] Y. Sun, X. Hou, J. Yang, H. Han, M. Su, and J. M. Guerrero, "New perspectives on droop control in AC microgrid," *IEEE Trans. Ind. Electron.*, vol. 64, no. 7, pp. 5741-5745, Jul. 2017.
[18] R. M. M. Pereira, C. M. M. Ferreira and F. M. Barbosa, "Comparative study of STATCOM and SVC performance on dynamic voltage collapse of an electric power system with wind generation," *IEEE Latin America Transactions*, vol. 12, no. 2, pp. 138-145, Mar. 2014.
[19] J. He, Y. Li, C. Wang, Y. Pan, C. Zhang, and X. Xing, "Hybrid microgrid with parallel- and series-connected microconverters," *IEEE Trans. Power Electron.*, vol. 33, no. 6, pp. 4817-4831, Jun. 2018.
[20] H. Geng, S. Li, C. Zhang, G. Yang, L. Dong, and B. N. Mobarakeh, "Hybrid communication topology and protocol for distributed-controlled cascaded H-Bridge multilevel STATCOM," *IEEE Trans. Ind. Appl.*, vol. 53, no.1, pp. 576-584, Jan./Feb.2017.